HAL
open science

Thermal camera-based fourier transform Infrared thermospectroscopic imager

Stéphane Chevalier, Jean-Noël Tourvieille, Alain Sommier, Jean-Christophe Batsale, Bruno Beccard, Christophe Pradère

To cite this version:

Stéphane Chevalier, Jean-Noël Tourvieille, Alain Sommier, Jean-Christophe Batsale, Bruno Beccard, et al.. Thermal camera-based fourier transform Infrared thermospectroscopic imager. Applied Spectroscopy, 2020, 75 (4), pp.462-474. 10.1177/0003702820973026 . hal-03307804

HAL Id: hal-03307804

https://hal.inrae.fr/hal-03307804v1

Submitted on 17 Jan 2022

HAL is a multi-disciplinary open access archive for the deposit and dissemination of scientific research documents, whether they are published or not. The documents may come from teaching and research institutions in France or abroad, or from public or private research centers.

L'archive ouverte pluridisciplinaire **HAL**, est destinée au dépôt et à la diffusion de documents scientifiques de niveau recherche, publiés ou non, émanant des établissements d'enseignement et de recherche français ou étrangers, des laboratoires publics ou privés.

Thermal Camera-Based Fourier Transform Infrared Thermospectroscopic Imager

Stéphane Chevalier[1], Jean-Noël Tourvieille[2], Alain Sommier[1], Jean-Christophe Batsale[1], Bruno Beccard[3], and Christophe Pradère[1]

Abstract

In this technical note, we present an advanced thermospectroscopic imager based on a Fourier transform infrared (FT-IR) spectrometer and a thermal camera. This new instrument can image both thermal emission and multispectral absorbance fields in a few seconds at a resolution of $4\,cm^{-1}$ or less. The setup is made of a commercial FT-IR spectrometer (ThermoFisher Nicolet iS50R) synchronized to an IR camera (indium antimonide and strained layer superlattice) as a detector to record the interferograms in each pixel of the images. A fast Fourier transform algorithm with apodization and Mertz phase correction is applied to the images, and the background is rationed to process the interferograms into the absorbance spectra in each pixel. The setup and image processing are validated using thin polystyrene films; during this processing, more than 1750 spectra per second are recorded. A spectral resolution equivalent to that of commercial FT-IR spectrometers is obtained for absorbance peaks valued less than two. The transient capability of the FT-IR thermospectroscopic imager is illustrated by measuring the heterogeneous thermal and absorbance fields during the phase change of paraffin over a few minutes. The complete mechanism of the thermochemical processes during a polymer solidification is revealed through the thermospectroscopic images, demonstrating the usefulness of such an instrument in studying fast transient thermal and chemical phenomena with an improved spectral resolution.

Keywords

Fourier transform infrared, FT-IR, spectroscopy, imaging, infrared, IR, calibration, paraffin

Introduction

Fourier transform infrared (FT-IR) spectroscopy with an array detector is an analytical technique that enables the molecular imaging of a complex sample in the mid-IR range.[1] Using this technique, based on the absorption of IR radiation through the vibrational transitions in covalent bonds, unique images with a high spatial resolution can be obtained. The quantitative information obtained from spectroscopic images is widely used in several domains such as the multispectral imaging of cells for cancer detection in biomedical applications,[2–5] identification of material crystals in earth science,[6] phase change of biopolymers,[7,8] and the investigation of electrochemical reactions in microreactive flows.[9–12] From the obtained multispectral images, local and quantitative information regarding the nature of the molecules in a sample can be clarified. Consequently, the development of such an apparatus is of importance for a large variety of scientific applications and technologies to enable faster, more precise, and versatile measurements of multispectral images at the microscale.

In the last decades, several groups have attempted to develop thermospectroscopic imagers that can record both thermal and spectral images for a range of infrared wavelengths. Romano et al.[13] reported on a

[1]I2M UMR 5295, Arts et Metiers Institute of Technology, CNRS, Université de Bordeaux, INRA, INP, HESAM Université, Talence, France
[2]Solvay, Laboratoire du futur, UMR 5258, Pessac, France
[3]Thermo Fisher Scientific, Courtaboeuf, France

Corresponding author:
Stephane Chevalier, Arts et Métiers ParisTech, Centre de Bordeaux-Talence Esplanade des Arts et Méties, Talence 33405, France.
Email: stephane.chevalier@u-bordeaux.fr

thermospectroscopic imager based on an indium antimonide (InSb) IR camera and a monochromator. Using a two-image method, the thermal images were separated from the spectral images. The instruments were reported to achieve an excellent signal-to-noise ratio (SNR) of 1000; however, they suffered from a lower spectral resolution compared to that of FT-IR spectrometers. A similar imager was developed by Ryu et al.[14] to study styrene radical polymerization, which represented the first attempt of formulating a noninvasive contactless method to determine both the chemical composition and temperature distribution. The utility of recording both thermal and spectral images was also demonstrated by Yamashita et al.[15] and Kakuta et al.,[16] with the aim of investigating the effect of temperature on the chemical mass transport in microfluidic chips, which makes thermospectroscopic imagers one of the most powerful tools for microfluidic contactless mass and heat transport characterizations.

Most of the previously reviewed works were based on thermospectroscopic imagers using monochromatic light from monochromatic filters or monochromator (by using a diffraction network). Although such a technology has been demonstrated to yield an excellent SNR, the spectral resolution is lower to that of FT-IR spectrometers; for instance, the resolution was approximately 20 nm in Romano et al.[13] compared to 2.5 nm (i.e., equivalent to a resolution of 4 cm^{-1}) for a classical FT-IR spectrometer. Furthermore, the measurement of one complete IR spectrum requires 3–5 min in the best reported cases,[13,17] which limits the use of monochromator for the slow transient regime involving a timescale of one hour or more or to systems in which a high spectral resolution is not required. Another solution was proposed by Lewis et al.[18] The authors used a FT-IR spectrometer with a focal plane array to image well-resolved absorbance spectra in chemicals dissolved in water. Going further in complex systems with multiphase flows, Chan and Kazarian[10] also used a commercial FT-IR spectrometer with an IR camera to measure the concentration gradient of two compounds dissolved in water. Such a result can only be achieved if the instrument can discriminate each peak of the component IR spectrum (in the limit of the intrinsic line width of the absorption bands), and thus improve the chemical analysis using chemometric techniques. Another example of the application of fast spectroscopic imaging was reported by Shalygin et al.,[19] who studied the transient chemical reaction of the precipitation process of oil asphaltenes. The authors could image the chemical reaction at different instants in 90 min. However, most chemical reactions span shorter times, which require a faster system using which a multispectral image can be obtained in less than 10s with a high spectral resolution of few cm^{-1}.

Few commercial spectrometer imagers exist, such as the Hyperion microscope from Bruker, which can satisfy the previously mentioned requirements. However, devices that can be applied in an open environment in which the operating conditions, such as temperature or pressure can be controlled or a complex setup (such as microfluidic reactors) can be introduced and imaged, have not been proposed yet. In addition, the existing commercial devices do not allow the simultaneous measurement of the sample surface temperature field. To fill this knowledge gap in the academic research community, a novel thermospectroscopic multispectral imager was developed. Specifically, in this technical note, we describe a new thermospectroscopic instrument based on a commercial ThermoFisher Nicolet iS50R FT-IR spectrometer combined with an IR camera to measure a complete IR spectrum and thermal field in less than 10s with high spectral and spatial resolutions, and we also provide to the academic community the open source code to process and analyze the IR interferograms.

To achieve such a temporal resolution, the spectrometers works in "rapid-scan" mode, in which the mirror of the interferometer moves at a constant optical retardation speed,[20] typically from 0.0633 cm/s to 0.3185 cm/s. A high-speed IR camera (frame rate higher than 400 Hz) is required to achieve a complete interferogram in a reasonable time. The ThermoFisher Nicolet iS50R spectrometer can also work in the "step-scan" mode, in which the mirror is held in a fixed position for a few milliseconds to image one point of the interferogram before moving to the next position. One advantage of the "step-scan" mode is the realization of a high SNR, as multiple images can be recorded at each mirror position (typically more than 100); however, the process to measure the entire wavelength range is considerably slower compared to that in the rapid-scan mode. Another advantage of the "step-scan" mode pertains to the imaging of fast transient phenomena, which are extremely repeatable like bursting phenomenon or high frequency periodic regime (see Brandstetter et al.[21] at the nanosecond scale for example). For this purpose, the transient phenomenon must be completely imaged in a few milliseconds at each mirror position. Each interferogram at each time scale is reconstructed afterward. However, this mode is not appropriate for minute scale transient phenomena. Thus, we selected the rapid-scan mode in line with the objective of enabling the instrument to record the image phenomena spanning over several minutes at a temporal resolution of a few seconds.

This technical note brings two major advances compared to the previous FT-IR imaging techniques: (i) how to combine state of the art cooled IR camera with commercial FT-IR spectrometer to make thermospectroscopic imaging (simultaneous measurement of thermal and absorbance fields) and (ii) the current advances of the IR camera make it possible to image fast transient multispectral phenomenon at the microscale.

Experimental Methods

Setup

In the spectrometer (a ThermoFisher Nicolet iS50R in this study), an IR beam is generated using a SiN source at 1480 K generating around 70 mW out of the interferometer. This beam is guided through a Michelson interferometer to generate the interferences by using a moving mirror. Subsequently, the modulated and collimated IR beam is led outside the spectrometers toward the optical table. The beam reaches a beam expander, which increases the area of the beam with a magnification of three to enable the imaging of large samples. The output IR beam from spectrometer is collimated with a divergence lower than 25 mrad and expanded using off axis parabolic mirrors and iris (spatial filtering). Subsequently, the beam crosses the sample, which is placed onto a calcium fluoride (CaF_2) wafer on a small heating plate to control the sample temperature, and later reaches the IR camera. Fig. 1a presents a schematic of the setup.

Two cameras were alternatively used in this study: a mid-wavelength infrared (MWIR) camera based on InSb sensor (FLIR SC7600 series) and a long-wavelength infrared (LWIR) camera based on strained layer superlattice (SLS) sensor (FLIR A6750 SLS). These cameras will be hereafter referred as the InSb and SLS camera. It is also important to note that while the SLS camera works in both the longwave and midwave infrared ranges, the biggest performance benefits can be obtained when it is filtered to the LWIR band exclusively. In fact, one of the key benefits of SLS is its short integration times (ITs), or snapshot speeds, compared to other infrared camera materials. Therefore, a versatile setup was developed where IR camera can be swapped easily to image within a specific spectral region of interest depending on both the thermal and chemical composition of the system.

Both the spectroscopic beam from the spectrometer source and the sample thermal emission beam are imaged by the camera. The sample thermal emission gives a measurement of the sample surface temperature. To separate these two values, a mechanical shutter is placed at the exit of the spectrometer to shut the spectroscopic beam and let the camera image only the sample thermal emission. The spectroscopic images are recovered by subtracting the thermal images. All the instruments are supervised using a LabVIEW interface to synchronize the mirror position in the spectrometer with the IR camera and control the heating plate temperature. A 3.5 V transistor–transistor logic (TTL) signal is generated by a data acquisition hardware. The TTL signal rising is triggered by the spectrometer when its mirror starts to move in the forward direction. This TTL is connected to the IR camera which records the images at the specified frame rate when the TTL signal is high. Once the whole interferogram is recorded by the IR camera, a signal is sent to close the mechanical shutter, which enables recording the thermal images. Figure 1b presents a schematic of the signal and connections used to synchronize all of the instrument parts. When

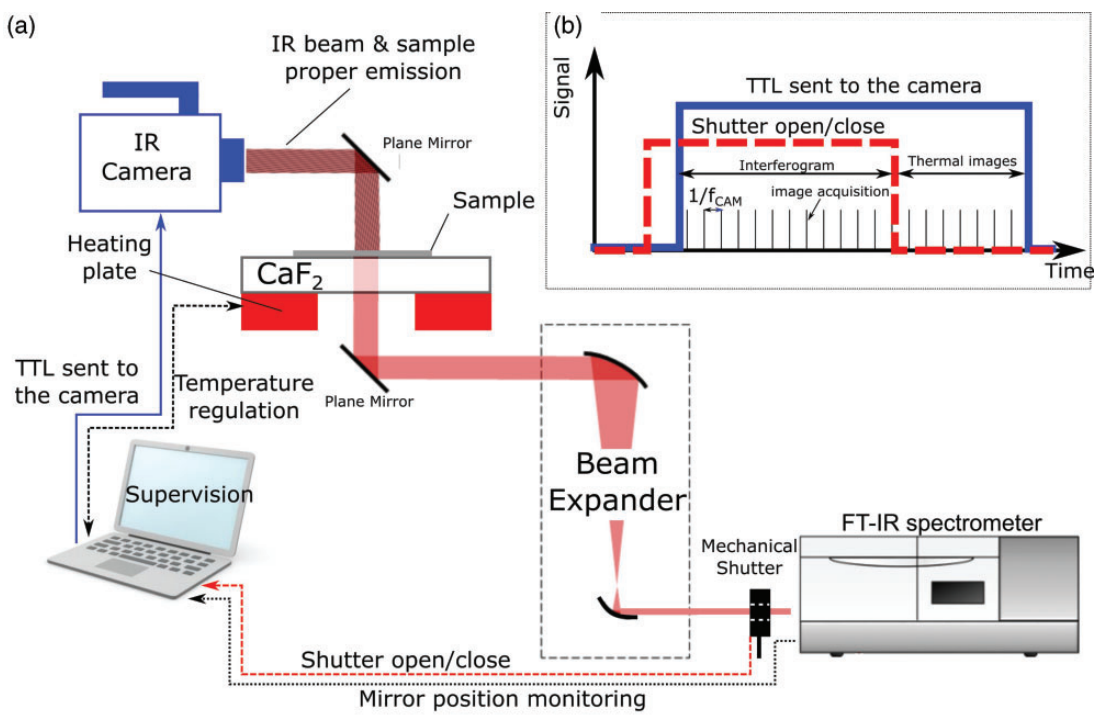

Figure 1. (a) Schematic of the fast thermospectroscopic imager. The IR camera can be either the InSB or SLS camera in this study. (b) Signal processing used to synchronize the instruments. IR: infrared; TTL: transistor–transistor logic; CaF_2: calcium fluoride.

the signal sent to the mechanical shutter is high, the shutter is open, and once the signal is low, the shutter is closed. Finally, by repeating this sequence, a complete interferogram and the associated thermal images are measured for ranges of sample temperatures and times.

Camera and FT-IR Setting

Several parameters of the camera and spectrometer need to be carefully set to ensure that the interferograms are correctly converted to IR spectra by using a fast Fourier transform (FFT). Depending on the spectrometer optical velocity in cm/s, V, and the maximum wavenumber of the IR spectrum, ν_{max}, the camera frame rate must satisfy the following inequality

$$f_{CAM} \geq 2\nu_{max}V \tag{1}$$

The factor of two is derived from the Nyquist criterion which states that the sampling frequency of the camera must be at least two times higher than the maximum frequency of the signal.[22] Consequently, based on the camera frame rate and the spectral resolution set in the spectrometer, the number of frames that must be recorded to ensure satisfactory sampling of the signal can be determined as follows

$$N_{frame} = \frac{2f_{CAM}}{res \times V'} \tag{2}$$

where res is the spectral resolution, i.e., $4\,\mathrm{cm}^{-1}$ in this study. The value of two in Eq. 2 is a result of the fact that double-sided interferograms are recorded and FFT is performed with no zero filling, which leads to a digital step that is one-half of the resolution, i.e., the digital step is $2\,\mathrm{cm}^{-1}$ for a spectral resolution of $4\,\mathrm{cm}^{-1}$. Finally, the time required to record one interferogram can be determined as

$$t = \frac{N_{frame}}{f_{CAM}} = \frac{2}{res \times V} \tag{3}$$

Interferogram Processing

The light intensity, $I_{tot}(x, y, \delta)$, recorded by the camera can be decomposed into three contributions: the sample thermal emission, $E(x, y)$, and the spectrometer source own emission comprising a steady DC component, $I_{dc}(x, y)$ and a modulated component, $I_{ac}(x, y, \delta)$, generated by the Michelson interferometer as following

$$I_{tot}(x, y, \delta) = E(x, y) + I_{dc}(x, y) + I_{ac}(x, y, \delta) \tag{4}$$

where δ is the optical retardation. The IR spectra will be obtained only from the I_{ac} contribution. To do so, the thermal images from the sample thermal emission, $E(x, y)$, are subtracted from the images recorded when the IR beam from the spectrometer passed though the sample. In this manner, two sets of images are obtained pertaining to thermal images and interferogram images free from the sample thermal emission.

The processing of an interferogram to obtain the IR spectrum is based on the methodology presented in Griffiths and De Haseth,[23] which is briefly summarized herein. The process is divided into two main steps illustrated in Fig. 2. In the step 1, as shown in Figs. 2a and 2b, the raw interferogram is apodized according to a Gaussian function as

$$I_a(x, y, \delta) = (I_{tot}(x, y, \delta) - E(x, y)) \times \exp\left(-\left(k\frac{N_{frame}}{N_{ref}}\delta^*\right)^2\right) \tag{5}$$

where I_a is the apodized interferogram, k is the apodization coefficient, N_{frams} is the number of images recorded, and $\delta^* = \delta \times res \in [-1; 1]$ is the dimensionless optical retardation. The reference number of images, N_{ref}, is arbitrarily set as 4111, which corresponds to the number of images needed for a resolution of $4\,\mathrm{cm}^{-1}$ and $\nu_{max} > 4000\,\mathrm{cm}^{-1}$. The apodization enables the reduction of the impact of noise on the IR spectrum. By adjusting the apodization

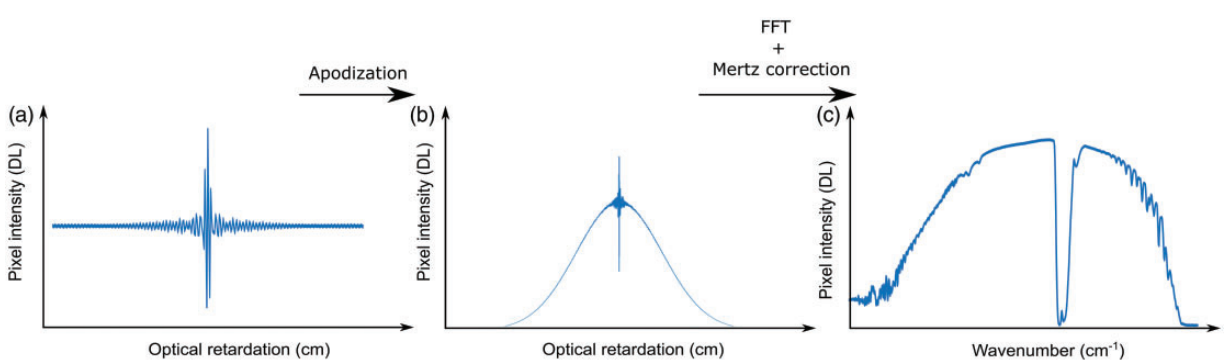

Figure 2. Summary of the processing algorithm from the interferogram to the IR spectrum. (a) Raw interferogram in one pixel of the camera. (b) Apodized interferogram. (c) IR spectrum in one pixel of the camera. FFT: fast Fourier transform; DL: digital level.

coefficient k, it is possible to "filter" more or less the signal from $k = 0$, in which the raw interferogram is maintained, to $k < 7$ for highly apodized interferograms in case of critical noise. Above a value of 7, it is empirically found that the IR spectrum started to be modified (attenuation of peaks, merging of peaks, etc.).

In step 2, as shown in Figs. 2b and 2c, a FFT algorithm is applied to the interferogram. Only the high frequency part of the resulting spectra is kept in order to eliminate the $I_{DC}(x,y)$ contribution at low frequency. Thus, the FFT acts both as a DC filter (high-pass filter) and IR spectrum computation as only the high frequency part of the signal is kept. Finally, the modulus of the IR spectrum is computed from the Mertz phase correction formula[1,23] as

$$S(x, y, \lambda) = \Re(S^*(x, y, \lambda)) \cos \Phi + \Im(S^*(x, y, \lambda)) \sin \Phi \tag{6}$$

where $S^*(x, y, \lambda)$ is the Fourier transform of $I_a(x, y, \delta)$, and $\Re$, $\Im$ and Φ denote the real part, imaginary part, and phase of S^*, respectively. A phase error occurs for a variety of reasons: systematic error in the measurement of the optical path difference, misalignment of the interferometer, or intrinsic asymmetry between the interferometer arms. These errors produce an interferogram that is asymmetric about its central maximum. The goal of any phase correction scheme is to recover, as far as is possible, the original spectrum. The same process is applied to each pixel of the image to obtain a multispectral image. The complete processing code is available in the following public repository: https://github.com/stephane-chevalier/FT-IR_imager

Absorbance Measurement Based on Camera IT Calibration

An important feature of quantum IR cameras is the IT, which needs to be carefully set: an excessively low value results in low camera sensitivity with a low SNR, whereas an excessively high value may result in a saturated signal. To solve this issue, Kirchner et al.[17] proposed the calibration of the camera IT to always ensure the highest camera sensitivity without saturation. In this work, the same methodology as described in Kirchner et al.[17] is applied to the IR spectrum to calibrate the camera IR. The methodology is briefly summarized as follows.

Classically, the absorbance of a sample is measured as the ratio of the background spectrum (without sample) to the sample spectrum for each pixel of the camera and each wavelength (or wavenumber) as

$$A(x, y, \lambda) = -\log_{10} \frac{S^s(x, y, \lambda)}{{}^b(x, y, \lambda)} \tag{7}$$

where $S^S(x,y,\lambda)$ and $S^b(x,y,\lambda)$ denote the IR spectra of the sample and background, respectively. However, to ensure the highest sensitivity of the absorbance measurements, it is advisable to use a different IT for the background and the sample, as the sample absorbs a considerably larger amount of the IR beam than the background does.[17] To this end, it is assumed that the pixel intensity of the IR spectrum, $S(x,y,\lambda)$, is a linear function of the IT, and the calibrated pixel intensity of the IR spectrum, $S_{cal}(x,y,\lambda)$ as follows

$$S(x, y, \lambda) = IT \times S_{cal}(x, y, \lambda) \tag{8}$$

The calibrated IR spectrum is obtained considering the least square from the N measurements of IR spectra at N ITs

$$S_{cal}(x, y, \lambda) = \left[\mathbf{x}^T\mathbf{x}\right]^{-1}\left[\mathbf{x}^T\mathbf{y}\right] \tag{9}$$

where $\mathbf{y} = [IT_1, IT_2, ..., IT_n]^T$ is the vector containing the range of IT considered, and $\mathbf{x} = [S^1(x,y,\lambda), S^2(x,y,\lambda), ..., S^n(x,y,\lambda)]^T$ is the vector containing the N pixel intensity of the IR spectra for each pixel at each wavelength. The calculation of $S_{cal}(x,y,\lambda)$ is done only for the background, and the absorbance of the sample for any camera IT is obtained as

$$A(x, y, \lambda) = -\log_{10} \frac{S^s(x, y, \lambda)}{IT^s \times S^b_{cal}(x, y, \lambda)} \tag{10}$$

where IT^S is the IT used for the sample. In this method, at least three or four background spectra must be measured for three or four ITs to obtain $S^b_{cal}(x, y, \lambda)$. Subsequently, the sample spectrum is imaged at a higher IT to enhance the SNR.

Results and Discussion

Thermospectroscopic Measurements

Camera IT Calibrations. The calibration was performed using both the InSb and SLS cameras. For each measurement, the same spectral resolution was set; however, the other parameters such as the spectrometer optical velocity or camera frame rate were adjusted according to the camera specifications (for example, spectral range or IT). All the employed setup parameters are summarized in Table I. A total of five or six ITs were chosen for each camera setup, and for each IT, three background interferograms were measured. Figs. 3a and 3b present a representative interferogram for a range of IT values. It can be observed that for a higher IT, i.e., 120 and 140 μs for the InSb camera, the signal is saturated, and the highest peak of the interferogram is not accurately measured. The same results can be observed for the SLS camera for an IT of 800 μs. The black body intensity is much lower in the LWIR range compared to the MWIR range which explained the larger SLS IT than the InSb one.

Table I. Experimental setup parameters for the two cameras.

Parameter	InSb	SLS
Spectral resolution (cm^{-1})	4	4
Spectral range (cm^{-1})	4000–1800	1400–850
Optical velocity (cm/s)	0.0633	0.1581
Measurement time (s)	7.90	3.16
Apodization coefficient	3	3
Camera frame rate (Hz)	510	450
Camera pitch (μm)	15	15
Pixel resolution	640 × 512	640 × 512

InSb: indium antimonide; SLS: strained layer superlattice.

The three interferograms recorded for each IT were processed to obtain the IR spectra which are then averaged to obtain a single spectrum. The resulting averaged spectra for each camera are presented in Figs. 3c and 3d. With an increase in the IT, the spectral intensity (expressed as digital level (DL)) per wavelength (or wavenumber) increases until a point, after which the value decreases (see the spectra at 120 and 140 μm in Fig. 3c, for example). This result is due to the pixel saturation on the interferograms, as observed previously. The saturation of the central interferogram peak impacts the entire spectrum in terms of the intensity; however, the shape seems to be preserved. The effect of saturation in the FT-IR imager is considerably

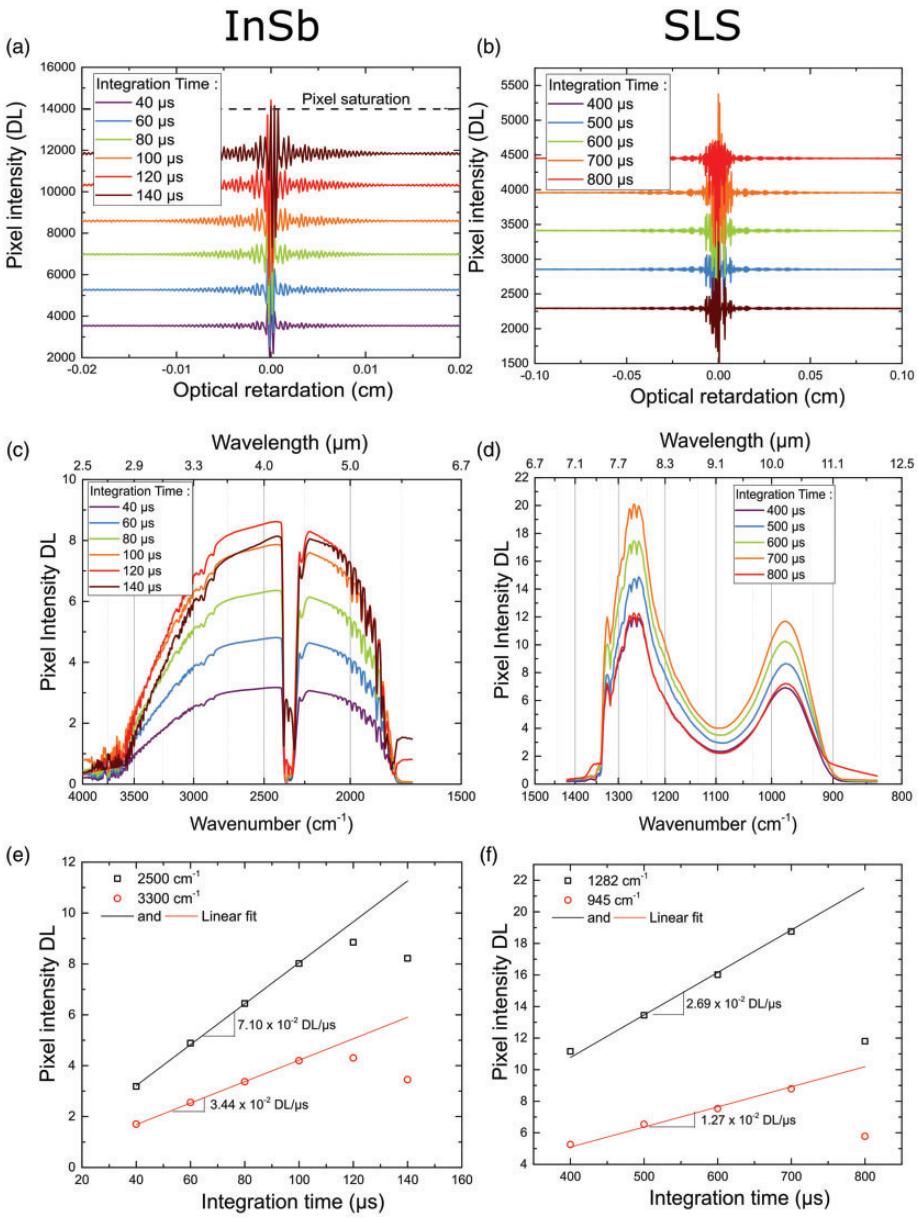

Figure 3. Calibration of the camera integration time using the background spectra. (a) and (b) Mean interferogram for a range of IT values. (c) and (d) Associated spectra obtained after the postprocessing. (e) and (f) Linear fit of the camera IT. InSB: indium antimonide; SLS: strained layer superlattice.

different from that of the saturation observed using a monochromator.[17]

Figs. 3e and 3f show the results of the camera IT calibration for two wavelengths. It is observed that the pixel intensity per wavelength varies linearly with the IT, as expected and recorded in previous studies.[13,17] This linear trend is visible for both cameras. However, for a higher IT, a deviation from linearity is observed due to the aforementioned effect of the saturation. The complete calibrated background spectrum, $S^b_{cal}S(x, y, \lambda)$, is obtained from the slope of the linear regression on the four first ITs, i.e., the linear regions in Figs. 3e and 3f. It is calculated for all the pixels of the image and all the wavelengths.

In the subsequent measurements, the camera IT was carefully set to avoid any saturation in all the pixels of the camera detector. This ensures the linear response of the detector, and therefore the correct amplitude in the IR spectrum.

Camera SNR Assessment

To evaluate the performances of the cameras in terms of the sensitivity, the SNR is computed from the IT background spectra. The SNR is defined as the ratio of the maximum average pixel intensity to the noise standard deviation (STD), i.e.,

$$SNR = \frac{\max\left(\bar{S}(\lambda)\right)}{STD(S(x, y, \lambda_{min}))} \tag{11}$$

where $\bar{S}$ is the spatial average of S, and $\lambda_{\min}$ is the wavelength (or wavenumber) at which the camera images only the noise, typically at 7.04 μm (1420 cm^{-1}) and 2.48 μm (4026 cm^{-1}) for the SLS and InSb camera, respectively. From the SNR, the minimum transmittance that can be measured can be deduced as $T_{min} = SNR^{-1}$, and the maximum absorbance is $A_{max} = \log_{10}(SNR)$. Table II summarizes the results of the SNR obtained for the two cameras by using the background spectra recorded with the highest IT before saturation, i.e., 120 μs and 800 μs for the InSb and SLS, respectively.

Table II. Noise assessment of the two cameras.

Parameter	InSb	SLS
Integration time (μs)	120	800
STD ($S_0(x,y,\lambda_{min})$) (DL)	0.14	0.09
$\max\left(\overline{S_0}(\lambda)\right)$(DL)	9.19	21.75
SNR	66	230
T_{min}	1.5×10^{-2}	0.4×10^{-2}
A_{max}	1.82	2.36

InSb: indium antimonide; SLS: strained layer superlattice; STD: standard deviation; DL: digital level.

It is observed that the SNR is approximately 66 for the InSb, whereas it is 230 for the SLS. These SNR values lead to an estimated maximum absorbance of approximately 1.8 and 2.4, respectively. Above this value, the signal is of the same order of magnitude as that of the camera noise. The apparent better sensitivity of the SLS camera compared to the InSb camera may be related to the longer IT used. Also, the energy par wavelength is higher for the SLS camera compared to the InSb one, which increases the SNR. This effect is due to the smaller spectral range (in terms of wavenumbers) of the SLS camera. And finally, the hardware of both cameras is also different and may explain the resulting sensitivity of these cameras.

To improve the SNR, it is advised to record more interferograms for each sample when possible or employ the "step-scan" mode in the spectrometer. However, in this case, the transient aspect of the measurements is lost or at least significantly reduced. Considering these aspects, a SNR of 1000 has been reported using a monochromator imager,[13] which indicates that if the temporal resolution is not a limiting factor, such an instrument can be used to measure monochromatic images with extremely low noise.

Comparison with Commercial FT-IR ThermoFisher Measurements

In this analysis, 38 and 76 μm thick polystyrene samples obtained from the NIST Laboratory were used to validate the thermospectroscopic imager. In these measurements, the polystyrene was maintained at the ambient temperature (no heating from the CaF_2 wafer). The calibrated backgrounds were imaged as described in the previous section, and the polystyrene samples were imaged using the experimental parameters described in Table I. Only the ITs were adjusted to increase the camera sensitivity when the IR beam passed through the sample, i.e., 130 and 180 μs for the InSb, and 800 and 900 μs for the SLS.

The results for the InSb camera are presented in Fig. 4. In Figs. 4a and 4b, the raw background and sample images, respectively (91 per 151 pixels), are shown for one mirror position. The intensity heterogeneities visible in Fig. 4a are due to tiny stains in the optics. Each pixel of the image includes complete interferogram, as shown in Fig. 4c. The background interferogram presents lower intensity than that of the sample, which is explained by the change in the IT for the sample measurements. This phenomenon is corrected when the interferograms are processed to obtain the IR spectra using the IT calibration. Fig. 4d shows that the sample spectrum has a lower intensity compared to that of the background spectrum, as expected. Finally, the IR absorbance is computed in each pixel for all the wavelengths to obtain a 3D multispectral absorbance image (see Fig. 4e). A similar result was obtained for the images obtained using the SLS camera.

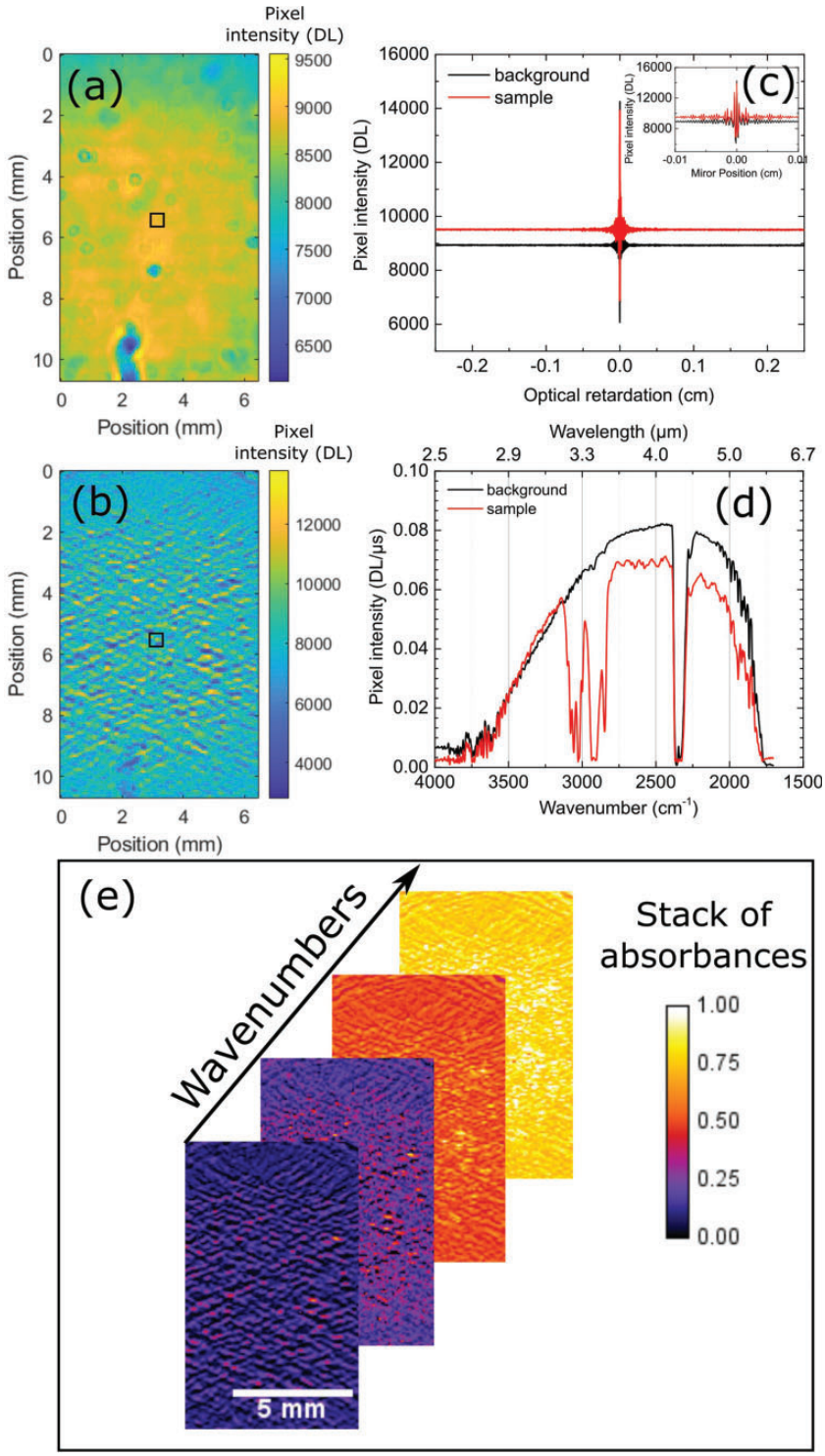

Figure 4. Data obtained before and after postprocessing of the interferograms. (a) Beam intensity of the background after the thermal emission removal. (b) Beam intensity after the thermal emission removal that passed through the polystyrene. (c) Interferograms of the black pixels in (a) and (b). (d) IR spectra obtained from the interferogram in (c). (e) Multispectral images of the sample absorbance obtained at the end of the postprocessing.

Subsequently, the polystyrene IR absorbance spectra obtained using the custom-made thermospectroscopic imager were compared to the IR absorbance spectra measured using the Nicolet iS50R spectrometer with the same resolution of 4 cm^{-1}. Each spectrum from the Nicolet spectrometer was a result of the average of 16 measurements. In contrast, each spectrum obtained from the cameras was a result of the average of all the pixels in the image.

Figures 5a to 5c show the results in which three IR absorbance spectra are presented for each polystyrene thickness, specifically corresponding to the InSb camera, SLS camera, and Nicolet spectrometer. An excellent agreement is observed between the spectra obtained using the thermospectroscopic imager and the spectra obtained using the commercial spectrometer, which validates the complete methodology (experimental setup, FFT postprocessing and calibration method) presented in this paper. In particular, the IR absorbance peaks are well located and correspond to the expected polystyrene signature reported in Danilaev et al.[24] The gap between 1800 and 1400 cm^{-1} may be seen as a disadvantage compared to commercial imaging spectrometer, but it is only limited by the spectral range of the camera. The instrument described here is fully versatile: any spectral range from near IR to LWIR can be targeted with the appropriate camera. The methodology will remain unchanged.

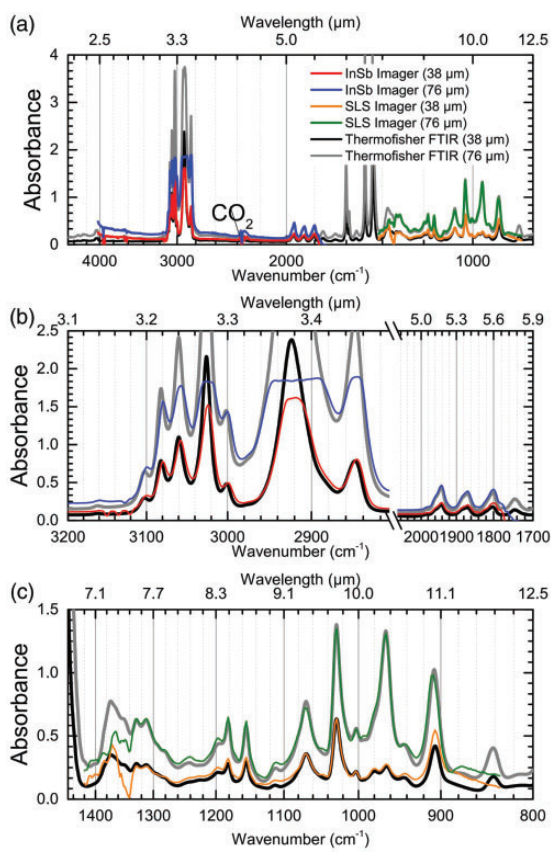

Figure 5. Comparison of the results between the FT-IR imager and a reference spectrum for the polystyrene samples. (a) Full spectra. (b) Focus in the 3.1–5.9 μm range. (c) Zoom in the 7.1–12.5 μm range.

In Fig. 5b, the absorbance peaks valued <2.0 absorbance units are well resolved. However, the peaks at 2950 cm^{-1} and 2850 cm^{-1} are saturated. This result is explained by the SNR analysis described in the previous subsection, which indicates that the absorbances more than 1.8 for the InSb cannot be correctly resolved because the signal is drowned into the noise. To increase this limit, more interferograms can be recorded, the black body intensity, $I_{tot}(x,y,\delta)$ increased, or the measurement can be switched to the step-scan mode to record hundreds of images at each mirror position, increasing the SNR. Noteworthy also is that the beam expender decreases the beam intensity that reaches the IR camera by a factor of 10. This also explains the rather low SNR observed in our measurements compared to some obtained from commercial setups.

By comparing the performance of the FT-IR thermospectroscopic imager to that of approaches using a monochromator as the IR source,[13,17] the following conclusions can be derived. The proposed setup enables the measurement of a complete IR absorbance spectrum in only a few seconds with an excellent spectral resolution. However, such a result involved a lower SNR than that reported in Kirchner et al.[17] Therefore, a balance must be maintained between the increased SNR realized using a monochromator and a reasonable spectral resolution with prompt measurement, which can be realized using the FT-IR spectrometer. This issue may be partially approached by using either a more sensitive camera or by performing the measurements in the "step-scan" mode to increase the SNR, although the experimental time would also be significantly increased in such a case.

Example of Application: Phase Change of a Paraffin

The solidification process of a paraffin (RT47, Rubitherm Technologies GmbH) was evaluated using the thermal camera-based thermospectroscopic imager. A liquid paraffin droplet was confined between two semi-transparent wafers with a 50 μm spacer to control the paraffin sample thickness. Full multispectral absorbance images and thermal fields (the surface sample thermal emission, $E(x,y)$ in camera DL) were recorded every 18 s from 50 to 40 °C using the InSb camera in the 4000–1600 cm^{-1} range. This delay between two measurements corresponds to the time needed to image the interferograms (<10s), plus the time needed by the camera to send the recorded images to the desktop (~5 s). The spectral resolution was set as 4 cm^{-1}, the optical velocity was set as 0.0633 cm/s and the camera frame rate was set to 507 Hz. The thermal fields were obtained from the average of 500 thermal images

recorded after each interferogram (once the mechanical shutter has been closed, see Fig. 1b). It is also reminded that the thermal images give only a measurement of the paraffin surface temperature, not from the bulk.

A total of 40 multispectral absorbances and thermal fields were recorded yielding more than seven Go of raw data (15 Go in total once the data were processed). The experiment spanned over 720 s (~12 min). The methodology described in the Experimental Methods section above was used to analyze the data. For the thermal field, the first thermal image recorded at 50 °C was taken as the reference, from which all the other thermal images are subtracted to observe only the relative variation in the temperature, because ΔT was linearly proportional to the pixel DL of the camera. In this case, an increase of the relative pixel intensity in DL is equivalent to a decrease of the sample relative temperature.

In Fig. 6, the thermospectroscopic images are presented as function of the experimental time and the heating plate temperature. Among the 1250 absorbance images recorded for each time slot, five of them are presented with the corresponding thermal image. The typical bands between 2918 and 2850 cm^{-1}, corresponding to the CH_2 vibrational mode and the images at 1800 and 3500 cm^{-1}, where the liquid paraffin is transparent, were chosen.

It can be seen that from 50 to 40 °C, when the temperature of the CaF_2 heating plate gets reduced to less than 45 °C, the solidification started, and the absorbance increased from 0 (liquid) to 0.5 or more (solid) at 1800 and 3500 cm^{-1}. This is mainly due to scattering by the solid paraffin. In contrast, the absorbance is observed to

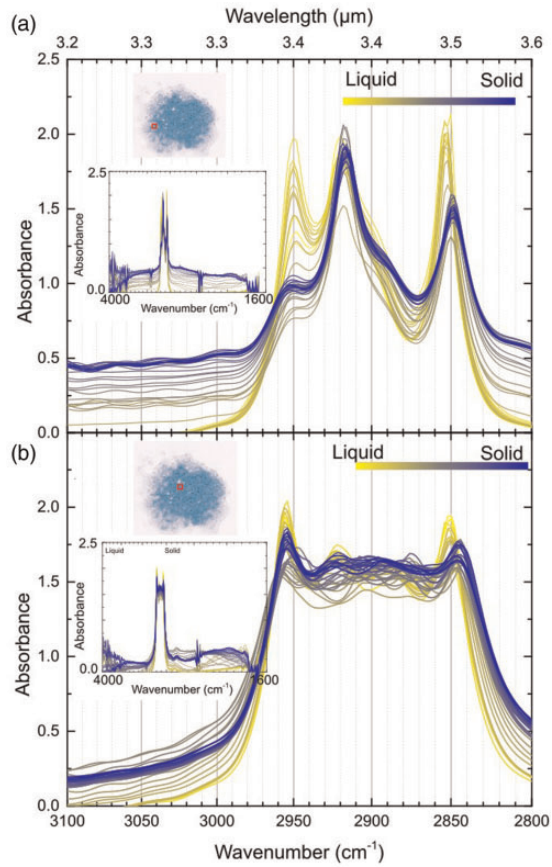

Figure 7. Paraffin absorbance spectra measured during the solidification for the two regions indicated in the image inserts (red square). (a) Left region and (b) central region. The inserted spectra show the entire range of measurement.

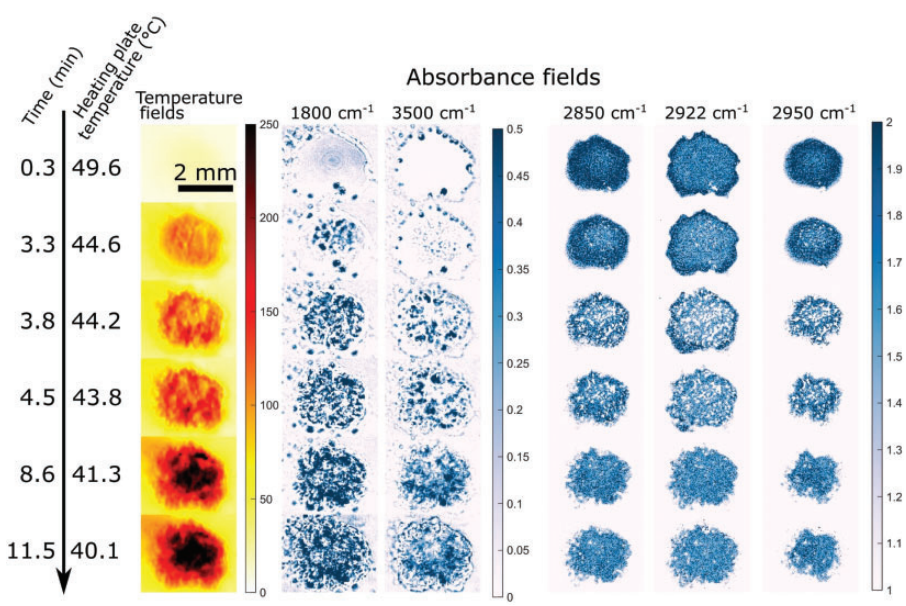

Figure 6. Temporal evolution of the paraffin multispectral absorbance and thermal fields. The relative temperature fields are in camera DL.

decrease from 2 to 1.5 in average at 2850, 2920, and 2950 cm^{-1} when the heating plate temperature was decreased. These results confirm that the thermotransmittance is wavelength dependent and can only be revealed with such multispectral images. In addition, it is interesting to note that the solidification kinetics was spatially heterogeneous, i.e., it started from the center and moved toward the sample boundary in a few minutes, as shown by the local variation of absorbance in each image.

In Fig. 6, it is also observed that the thermal field presented the same heterogeneities as the absorbance field. This finding indicates that when the solidification starts, a certain quantity of latent heat is released, which increases the temperature locally. All these results correspond to the extensive analysis of thermochemical processes, which can be realized simultaneously using the newly developed thermal camera-based thermospectroscopic imager.

An in-depth analysis of the spectral information of the paraffin was performed through the Figs. 7 and 8. In Fig. 7, the IR paraffin spectra for a range of heating plate temperature are presented from two sample regions, i.e., the central region where the paraffin thickness is 50 μm and the boundary region where the thickness is lower to 50 μm. Each spectrum results from an average of 25 spectra located in the 5×5 pixel region designated by the red square in the inserted image. The expected spectral signature of the paraffin used was similar to that of the RT80 wax reported in Fuensanta et al;[25] in particular, the typical bands at 2918 and 2847 cm^{-1} correspond to the CH_2 stretching, respectively, antisymmetric and symmetric modes. From liquid to solid, the IR spectra were significantly affected, both in terms of absorbance value (as already seen through Fig. 6), but also in terms of CH_2 peak position. Such variations are clearly visible in Fig. 7a with very well-defined peaks. In comparison, Fig. 7b exhibits saturated peaks in the vibrating CH_2 band. Such differences are explained by the camera SNR (see the Camera SNR Assessment section), which hinder the measurement of absorbance greater than 2. In Fig. 7a, a thinner paraffin layer was used which ensured a lower absorbance and therefore well-defined absorbance peak in the CH_2 vibration band. However, the saturated peaks in Fig. 7b shows a similar behavior (see at 2955 and 2847 cm^{-1}) in which a decrease of the absorbance with the temperature can be observed.

The results presented in Fig. 7a are analyzed versus the heating plate temperature in Fig. 8 for the characteristic CH_2 vibrating bands. The spectral signature of the paraffin corresponds to the results reported in the existing literature, in which the CH_2 stretching modes were found to be

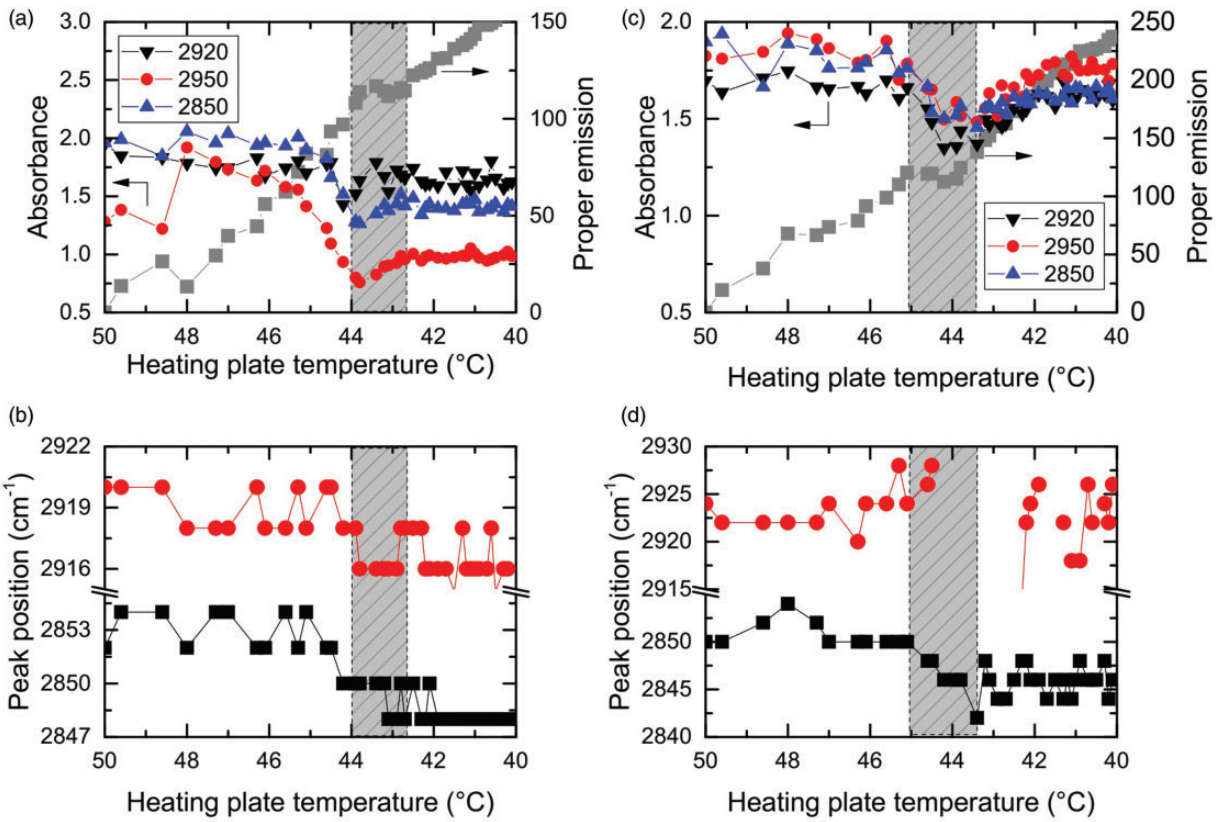

Figure 8. Effect of the sample temperature change on peak absorbance, peak position, and thermal emission in the left region depicted in Fig.7a. (a) Maximum peak absorbance and thermal emission and (b) peak position.

thermally dependent both in terms of magnitude and wavelength.[7,26] In Fig. 8a, one can observe that the absorbance of the paraffin decreases from the liquid (hot conditions) to solid (cool conditions) state. In particular, the phase change is visible both in terms of absorbance brutal changes (strong decrease and increase before stabilization), but also in terms of thermal emission with the existence of a plateau (grey zone) between 44 and 42.7 °C. One explanation can rise from the release of latent heat during the solidification process which may balance the sample cooling.

In Fig. 8b, the locations change of the 2850 and 2920 cm^{-1} peaks are presented. Both the CH_2 stretching peaks shifted by approximately 5 cm^{-1} when the paraffin temperature decreased, as reported in the literature; specifically, a similar shift (5 cm^{-1}) was reported by Merk et al.[7] considering bioparaffins. An uncertainty of $\pm 2\,cm^{-1}$ is found in our measurements which is enough to reveal such small peaks position shift. This result illustrates the accuracy of the thermospectroscopic imager in detecting small peak shifts (few cm^{-1}) in the sample. Such an accuracy, both in terms of spectral and temporal resolution, cannot be achieved using an IR monochromator.

Conclusion

This technical note describes the development of a fast thermospectroscopic imager based on thermal camera and a commercial FT-IR spectrometer. All the aspects in terms of the experimental setup, processing of the interferograms to obtain the IR spectra, and background calibration technique to enhance the sensitivity of the measurements are described. A complete multispectral image (91 per 151 pixels) in addition to the thermal field can be recorded within 3–7 s, depending on the experimental settings (such as the spectral resolution, or the optical velocity). Such a result corresponds to the measurement of 1750 spectra per second, which makes this new imager the fastest one in the research community.

This new apparatus is not only fast but also as accurate as a commercial FT-IR spectrometer in terms of the spectral resolution. This result was validated using several polystyrene samples and several IR cameras as detectors to cover a large range of wavelengths, e.g., between 4000 and 1700 cm^{-1} (corresponding to 2.5–5.6 μm) and between 1400 and 850 cm^{-1} (corresponding to 7–12 μm). Furthermore, it was demonstrated that the absorbance peaks can be well resolved as long as the absorbance is <2. This limit occurs due to an SNR of approximately 100 which is partly due to the decrease of the beam intensity resulting from the beam expansion. Several approaches can be employed to improve the apparatus SNR to achieve a higher performance in terms of transmittance through a highly opaque medium.

The usefulness of measuring both multispectral and thermal images was illustrated through the phase change of a paraffin. The spatial heterogeneities were clearly observed during the solidification in both the absorbance and thermal fields. Each pixel of the image contained an IR spectrum and the information concerning the local material temperature. Therefore, it was possible to follow the complete thermochemical process of solidification through the variation of the heat released and increase in absorbance in each pixel of the image every 18 s. In addition, extremely small variations in the peak wavelength shifts (approximately 5 cm^{-1}) were observed during the temperature changes, as expected according to the existing literature. This phenomenon demonstrates the higher accuracy of the proposed instrument in terms of the spectral resolution compared to that of the thermospectroscopic imagers using an IR monochromator.

A limitation of such multispectral imaging is the large quantity of data generated for each measurement. The complete measurements of the paraffin solidification produced more than 15 Go of data (approximately 1 Go/min) once all the images were processed. With the development of new imaging techniques, big data management is expected to become a prominent issue that needs to be addressed.

Acknowledgments

ADEME is gratefully acknowledged by the authors for its support through the project IGAR.

Declaration of Conflicting Interests

The author(s) declared no potential conflicts of interest with respect to the research, authorship, and/or publication of this article.

Funding

The author(s) received no financial support for the research, authorship, and/or publication of this article.

ORCID iD

Stephane Chevalier https://orcid.org/0000-0002-4614-1867

Supplemental Material

All supplemental material mentioned in the text, consisting of a nomenclature table, is available in the online version of the journal.

References

1. P.R. Griffiths. "Fourier Transform Infrared Spectrometry". Science. 1983. 222(4621): 297–302.
2. K.L.A. Chan, S.G. Kazarian. "Aberration-Free FTIR Spectroscopic Imaging of Live Cells in Microfluidic Devices". Analyst. 2013. 138(14): 4040–4047.
3. G. Birarda, G. Grenci, L. Businaro, et al. "Fabrication of a Microfluidic Platform for Investigating Dynamic Biochemical Processes in Living Samples by FTIR Microspectroscopy". Microelectron. Eng. 2010. 87(5–8): 806–809.

4. H.J. Butler, P.M. Brennan, J.M. Cameron, et al. "Development of High-Throughput ATR-FTIR Technology for Rapid Triage of Brain Cancer". Nat. Commun. 2019. 10(1): 4501.
5. N. Kaun, S. Kulka, J. Frank, et al. "Towards Biochemical Reaction Monitoring Using FT-IR Synchrotron Radiation". Analyst. 2006. 131(4): 489–494.
6. G. Della Ventura, F. Bellatreccia, A. Marcelli, et al. "Application of Micro-FTIR Imaging in the Earth Sciences". Anal. Bioanal. Chem. 2010. 397(6): 2039–2049.
7. S. Merk, A. Blume, M. Riederer. "Phase Behaviour and Crystallinity of Plant Cuticular Waxes Studied by Fourier Transform Infrared Spectroscopy". Planta. 1997. 204(1): 44–53.
8. M. Romano, M. Ryu, J. Morikawa, et al. "Simultaneous Microscopic Measurements of Thermal and Spectroscopic Fields of a Phase Change Material". Infrared Phys. Technol. 2016. 76: 65–71.
9. C. Chan, N. Zamel, X. Li, et al. "Experimental Measurement of Effective Diffusion Coefficient of Gas Diffusion Layer/Microporous Layer in PEM Fuel Cells". Electrochim. Acta. 2012. 65: 13–21.
10. K.L.A. Chan, S.G. Kazarian. "FT-IR Spectroscopic Imaging of Reactions in Multiphase Flow in Microfluidic Channels". Anal. Chem. 2012. 84(9): 4052–4056.
11. A. Perro, G. Lebourdon, S. Henry, et al. "Combining Microfluidics and FT-IR Spectroscopy: Towards Spatially Resolved Information on Chemical Processes". React. Chem. Eng. 2016. 1(6): 577–594.
12. B.A. Rizkin, F.G. Popovic, R.L. Hartman. "Review Article: Spectroscopic Microreactors for Heterogeneous Catalysis". J. Vac. Sci. Technol. A. 2019. 37(5): 050801.
13. M. Romano, C. Ndiaye, A. Duphil, et al. "Fast Infrared Imaging Spectroscopy Technique (FIIST)". Infrared Phys. Technol. 2015. 68: 152–158.
14. M. Ryu, J.A. Kimber, T. Sato, et al. "Infrared Thermo-Spectroscopic Imaging of Styrene Radical Polymerization in Microfluidics". Chem. Eng. J. 2017. 324: 259–265.
15. H. Yamashita, N. Kakuta, D. Kawashima, et al. "Measurement of Temperature-Dependent Diffusion Coefficients of Aqueous Solutions by Near-Infrared Simultaneous Imaging of Temperature and Concentration". Biomed. Phys. Eng. Express. 2018. 4(3): 035030.
16. N. Kakuta, H. Yamashita, D. Kawashima, et al. "Simultaneous Imaging of Temperature and Concentration of Ethanol–Water Mixtures in Microchannel Using Near-Infrared Dual-Wavelength Absorption Technique". Meas. Sci. Technol. 2016. 27(11): 115401.
17. S. Kirchner, S. Narinsamy, A. Sommier, et al. "Calibration Procedure for Attenuation Coefficient Measurements in Highly Opaque Media Using Infrared Focal Plane Array (IRFPA) Spectroscopy". Appl. Spectrosc. 2018. 72(2): 177–187.
18. E.N. Lewis, P.J. Treado, R.C. Reeder, et al. "Fourier Transform Spectroscopic Imaging Using an Infrared Focal-Plane Array Detector". Anal. Chem. 1995. 67(19): 3377–3381.
19. A.S. Shalygin, I.V. Kozhevnikov, S.G. Kazarian, et al. "Spectroscopic Imaging of Deposition of Asphaltenes from Crude Oil Under Flow". J. Pet. Sci. Eng. 2019. 181: 106205.
20. E.Y. Jiang. "Advanced FT-IR Spectroscopy: Principles, Experiments, and Applications Based on Research-Grade Nicolet FT-IR Spectrometers". 2003. www.scribd.com/document/91792213/Advanced-FTIR-Spectroscopy [accessed Oct 21 2020]..
21. M. Brandstetter, A. Genner, C. Schwarzer, et al. "Time-Resolved Spectral Characterization of Ring Cavity Surface Emitting and Ridge-Type Distributed Feedback Quantum Cascade Lasers by Step-Scan FT-IR Spectroscopy". Opt. Express. 2014. 22(3): 2656.
22. P.R. Griffiths, J.A. De Haseth. "Sampling the Interferogram". Fourier Transform Infrared Spectrometry. Hoboken, NJ: John Wiley and Sons, Inc., 2006. Chap. 3, Pp. 57–74.
23. P.R. Griffiths, J.A. De Haseth. "Fourier Transforms". Fourier Transform Infrared Spectrometry. Hoboken, NJ: John Wiley and Sons, Inc., 2006. Chap. 4, Pp. 75–95.
24. M.P. Danilaev, E.A. Bogoslov, O.G. Morozov, et al. "Obtaining Carbon Dendrites from the Products of Conversion of Polymer Materials". J. Eng. Phys. Thermophys. 2015. 88(3): 774–780.
25. M. Fuensanta, U. Paiphansiri, M.D. Romero-Sánchez, et al. "Thermal Properties of a Novel Nanoencapsulated Phase Change Material for Thermal Energy Storage". Thermochim. Acta. 2013. 565: 95–101.
26. R.M. Roehner, F.V. Hanson. "Determination of Wax Precipitation Temperature and Amount of Precipitated Solid Wax Versus Temperature for Crude Oils Using FT-IR Spectroscopy". Energy Fuels. 2001. 15(3): 756–763.